SCIENCE CHINA
Technological Sciences

Special Issue: Celebrating the 70th Anniversary of *Science China*
•Review•

July 2020 Vol.63 No.7: 1110–1126
https://doi.org/10.1007/s11431-019-1503-0

Periodically poled $LiNbO_3$ crystals from 1D and 2D to 3D

WANG TianXin, CHEN PengCheng, XU Chuan, ZHANG Yong*, WEI DunZhao, HU XiaoPeng, ZHAO Gang*, XIAO Min & ZHU ShiNing*

National Laboratory of Solid State Microstructures, College of Engineering and Applied Sciences, and School of Physics, and Collaborative Innovation Center of Advanced Microstructures, Nanjing University, Nanjing 210093, China

Received November 8, 2019; accepted December 12, 2019; published online May 11, 2020

A periodically-poled $LiNbO_3$ (PPLN) crystal features space-dependent second-order nonlinear coefficients, which is one of the most important materials to effectively control nonlinear optical interactions through quasi-phase matching (QPM). By using electric-field poling method, 1D and 2D PPLN crystals have been successfully fabricated for laser frequency conversion, quantum light sources, nonlinear beam shaping and nonlinear optical imaging. Recently, femtosecond laser engineering technique is utilized to prepare 3D domain structures inside $LiNbO_3$ crystal, which provides a promising platform to control nonlinear interacting waves in 3D configuration. After 40 years of developments, PPLN crystals still have exciting prospects in fundamental researches and practical applications for integrated photonic chip, quantum information processing, and so on.

periodically-poled $LiNbO_3$, quasi-phase matching, nonlinear optics

Citation: Wang T X, Chen P C, Xu C, et al. Periodically poled $LiNbO_3$ crystals from 1D and 2D to 3D. Sci China Tech Sci, 2020, 63: 1110–1126, https://doi.org/10.1007/s11431-019-1503-0

1 Introduction

In 1960, Maiman et al. [1] presented the first ruby laser, which features high peak power, outstanding coherence and monochromatic properties. Soon after that, Franken et al. [2] injected a ruby laser into quartz samples. A blue spot appeared and second-harmonic generation (SHG) was observed, which opened the era of nonlinear optics. By use of nonlinear optical frequency conversions, such as SHG, sum-frequency generation (SFG), difference-frequency generation (DFG), optical parametric oscillation (OPO) and optical parametric amplification (OPA), new laser sources that were not previously available could now be obtained. However, because of the dispersive nature of crystals, the phases of the fundamental wave and the newly generated nonlinear wave could not remain consistent during propagation, which results in a low conversion efficiency. To compensate the phase mismatch, the birefringence phase matching (BPM) technique was first proposed, in which the angular or temperature dependence of the crystal birefringence is utilized to cancel the phase mismatch. However, BPM is not suitable in several popular nonlinear crystals including $LiNbO_3$ crystal because of small birefringence.

In 1962, the QPM theory was proposed [3,4], in which the spatial modulation of $\chi^{(2)}$ is used to satisfy the phase matching condition. PPLN crystal is one of the most popular crystals for QPM. Consider SHG in a one-dimensional (1D) PPLN crystal as an example (Figure 1(a)). The reciprocal lattice vector (RLV) is $G_m=2\pi m/\Lambda$ with Λ being the poling period. The QPM condition can be written as $2\mathbf{k_1}+\mathbf{G_m}=\mathbf{k_2}$ (Figure 1 (b)). According to the Fourier transform, when the duty cycle of the domain structure is 0.5, the intensity of the corresponding RLV is $2/m\pi$. Clearly, the first-order RLV has

*Corresponding authors (email: zhangyong@nju.edu.cn; zhaogang@nju.edu.cn; zhusn@nju.edu.cn)

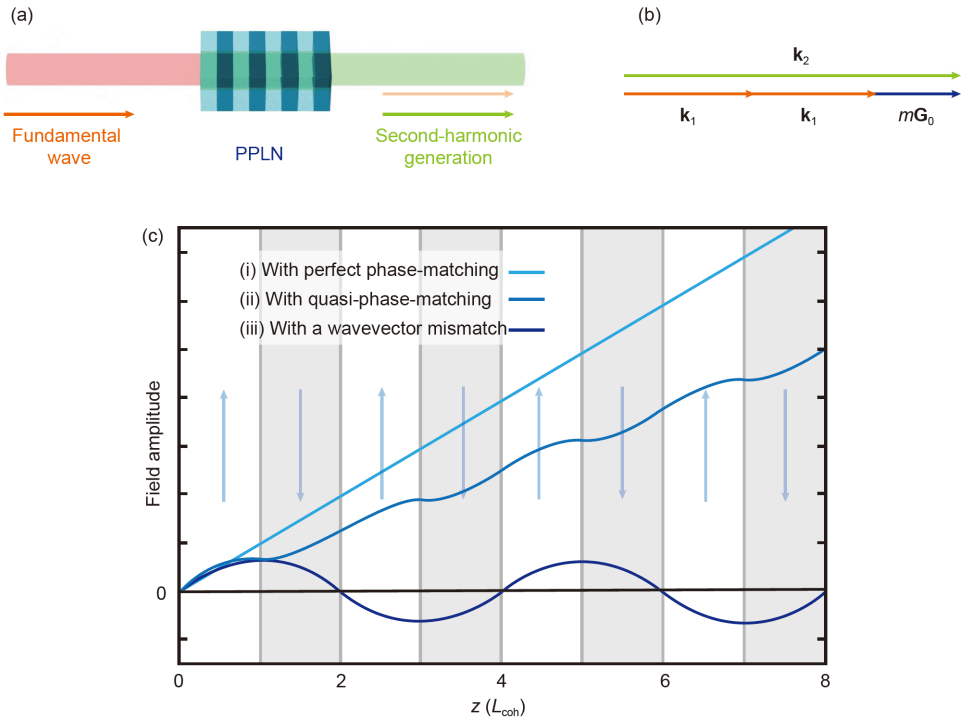

Figure 1 (Color online) (a) SHG process in a PPLN crystal; (b) phase-matching diagram of QPM; (c) second harmonic (SH) intensities as functions of propagation distance with (i) perfect phase-match, (ii) QPM, and (iii) no phase match.

the largest Fourier coefficient. In comparison with BPM, QPM offers several unique advantages. First, the largest nonlinear coefficient d_{33} can be used under QPM configuration. Second, QPM can be applied in many nonlinear optical crystals that are not suitable for BPM. Third, the spatial walk-off effect can be avoided with QPM technique.

The experimental breakthrough was made by Ming et al. [5] and Feng et al. [6] in 1980, who successfully prepared PPLN crystals with growth striation technique. Since then, PPLN crystal (also called optical superlattice and nonlinear photonic crystal) has been one important material in the field of nonlinear and quantum optics. Now, the general way to fabricate a PPLN crystal is the electric field poling (EFP) method, in which the ferroelectric domains are selectively inverted by applying an external electric field [7]. Researches have also developed chemical indiffusion [8,9], scanning force microscopic poling [10] and electron-beam poling [11], which have been applied for specific circumstances such as PPLN waveguides, surface poling and short-pitch poling. Especially, the recent advances in femtosecond laser engineering method make it possible to fabricated 3D domain structure inside a $LiNbO_3$ crystal [12,13]. Its function has been significantly enlarged from laser frequency conversion to nonlinear beam shaping, nonlinear imaging, nonlinear holography and quantum sources.

In addition to the traditional QPM in Figure 1(b), novel phase-matching configurations such as nonlinear Cerenkov radiation, nonlinear Bragg diffraction and nonlinear Raman-Nath diffraction are proposed and realized in PPLN crystals (Figure 2(b)–(d)). In a Cerenkov-type SHG process, the second-harmonic waves emit along an angle of θ (Figure 2 (b)). The phase matching condition satisfies $|\mathbf{k_2}| \cdot \cos\theta = 2|\mathbf{k_1}|$ [14–22]. Cerenkov-type SHG can be enhanced by the domain walls in PPLN crystal [23, 24], which has been further applied in 3D domain imaging [25,26]. In a PPLN wave-

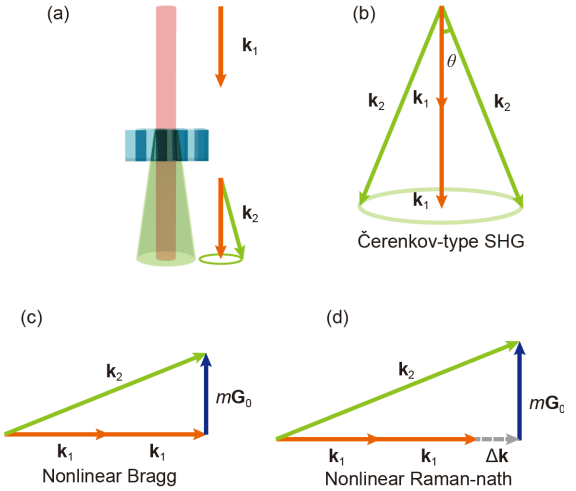

Figure 2 (Color online) (a) Schematic diagram of Cerenkov-type SHG; (b) phase-matching configuration of Cerenkov SHG; (c) phase-matching configuration of nonlinear Bragg diffraction; (d) phase-matching configuration of nonlinear Raman-Nath diffraction. $\mathbf{k_1}$ is the fundamental wave vector, $\mathbf{k_2}$ is the SH wave vector, $m\mathbf{G_0}$ is the RLV and $\Delta\mathbf{k}$ is the wave vector mismatch.

guide, QPM Cerenkov SHG, SFG and third-harmonic generation (THG) have been experimentally demonstrated [27–29], in which the emit angle can be modulated by the RLVs. Interestingly, scattering can involve in a QPM Cerenkov process and produce a SH arc pattern [30]. In the nonlinear Raman-Nath diffraction, phase matching requires $|\mathbf{k_2}| \cdot \sin\alpha_m = m|\mathbf{G_0}|$ [31,32]. In nonlinear Bragg diffraction, the phase matching condition is $\mathbf{k}_2 = 2\mathbf{k_1} + m\mathbf{G_0}$ [33]. Generally, the intensity of Cerenkov SHG grows with interaction distance because the longitudinal phase matching condition is satisfied. In contrast, the SH signal in a nonlinear Raman-Nath diffraction oscillates with the distance. Generally, in comparison to Cerenkov-type and Raman-Nath-type SHG, nonlinear Bragg configuration is more efficient since it satisfies both longitudinal and transverse phase matching condition.

In this review, we briefly review the development of PPLN fabrication techniques in Sect. 2. In Sect. 3, we focus on the applications of 1D PPLN crystals in laser frequency conversion and quantum sources. In Sect. 4, we discuss the applications of 2D PPLN crystals in nonlinear beam shaping and quantum light sources. In Sect. 5, we address nonlinear optical imaging techniques of domain structures. And in Sect. 6, we introduce the recent development of 3D domain structure and its applications in nonlinear beam shaping. Note that other popular periodically poled crystals such as PPLT and PPKTP are also addressed because they work in a similar way for QPM-based applications.

2 Fabrication techniques

2.1 Crystal growth and doping techniques

In the growth striation technique [6], the PPLN crystal is fabricated using a Czochralski growth system. The melt is properly doped to control the domain structure. The commonly used dopants include yttrium, indium and chromium. The typical concentration is 0.1 wt.%−0.5 wt.%. The growth striations are fabricated during the crystal growth process by introducing temperature fluctuations between the solid-liquid interfaces or an alternating current [34]. The gradient of the doping concentration is controlled to be negative (or positive) to produce a positive (or negative) domain region [35]. Island-like domain structure and non-uniform domain width may appear during crystal growth, which can be solved by carefully optimizing the experimental parameters such as the current pulse duration. This technique has been successfully applied to grow periodic structures in various nonlinear crystals (including $LiNbO_3$, $LiTaO_3$ [36], barium sodium niobate (BSN) [37], and triglycine sulfate (TGS) [38]) and single-crystal fibers [39,40]. The growth striation technique has unique advantage to produce PPLN crystals with large cross-sections, which are very useful for frequency conversion of high power laser.

Interestingly, it is convenient to dope certain laser active ions during the crystal growth. For example, Nd^{3+} and Er^{3+} have been successfully doped in PPLN crystal [8,9], which has potential applications in self-frequency-doubling laser. In addition, chemical doping and ion exchange can realize domain inversion in $LiNbO_3$ crystals. In 1979, Miyazawa et al. [41] found that in the 900°C–1100°C range, a $LiNbO_3$ single crystal with a titanium (Ti)-doped $+z$ plane formed a domain reversal layer. In 1995, Zhu et al. [42] also confirmed that the use of proton or ion exchange followed by heat treatment could produce domain inversion on the $+z$ plane of $LiNbO_3$ crystal. Because domain inversion caused by chemical doping and ion exchange only occurs within a few micrometers of the surface of crystals [42], this technique has been applied to fabricate optical waveguides with periodic domain structures [43–46]. High efficiency SHG was obtained in a periodically poled optical waveguide device because of the tight beam confinement [47].

2.2 Electric field poling

Figure 3(a) shows a typical external EFP device. Generally, it uses a patterned electrode on the crystal's $+z$ surface via ultraviolet (UV) lithography and a planar electrode on the

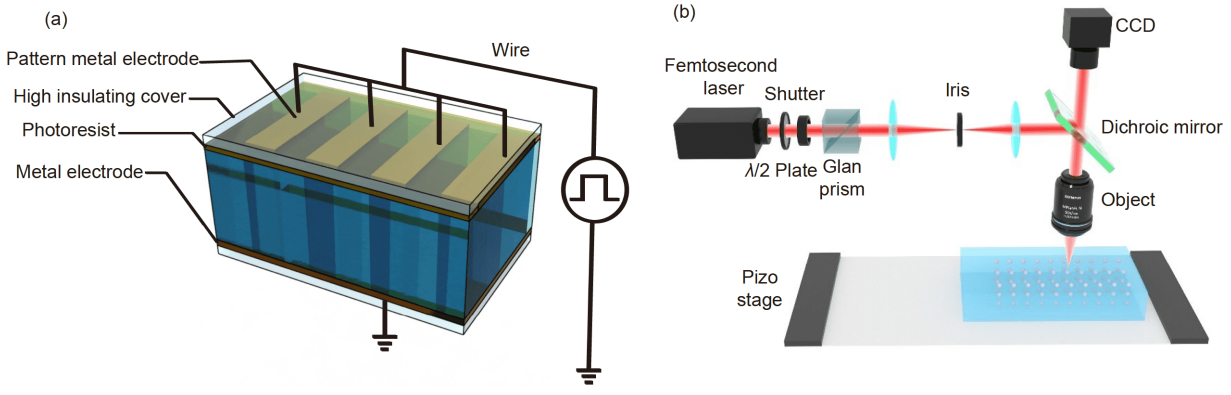

Figure 3 (Color online) (a) Schematic setup for the EFP technique; (b) typical experimental setup for femtosecond laser direct writing technique.

crystal's $-z$ surface. A voltage that is higher than the coercive field is applied to produce the domain reversal structure; in this way, the electrode pattern determines the domain structure directly. Using the EFP technique, periodic domain structures have been successfully achieved in $LiNbO_3$, $LiTaO_3$ [48], potassium titanyl phosphate ($KTiOPO_4$) [49,50] crystals. In 1995, researchers used the EFP technique to fabricate PPLN crystals with diameters of up to 3 inches [51]. In 1999, a backswitching method was developed to produce a PPLN crystal with a structure period of 4 μm for the generation of 460 nm blue light [52]. Later, Busacca et al. [53,54] used the intentional overpoling step to produce a domain period of approximately 1 μm on the crystal surface. Generally, the poling period ranges from a few microns to 30 μm and the crystal thickness is ~1 mm. To further improve these parameters of PPLN crystal, one has to overcome high coercive field and domain widening effect. The coercive field of a MgO-doped $LiNbO_3$ crystal is decreased significantly in comparison with the non-doped one [55] while its optical damage threshold is enhanced by two orders of magnitude. The thickness of the produced MgO:PPLN crystals reaches 5 mm in 2005 [56] and 10 mm in 2012 [57]. Meanwhile, the period of MgO:PPLN crystal has reached 1.4 μm by using a multi-pulse poling technique [57].

Currently, it is still difficult to achieve a PPLN crystal with sub-micron domain structure. The main reason is that sideways growth occurs when the domains are reversed under the surface electrodes [58,59]. Because the external electric field is normally oriented in the z-direction, it is inconvenient to electrically pole x- or y-cut crystals.

2.3 Electron and ion beam poling

In 1990s, researchers attempted to use an electron beam to write on the surfaces of nonlinear crystals to form domain reversal structures [11]. This technique uses a scanning electron microscope (SEM) as the electron beam source; the position of the electron beam was controlled to enable writing of a specific pattern. The $LiNbO_3$ crystal was mounted on the SEM sample stage and a high-energy electron beam was focused on its $-z$ plane. The penetration depth generally extends to only a few micrometers, but the domain inversion can be stably extended through the entire thickness of the sample (typically ~1 mm). Mizuuchi et al. [60] reported the ion beam exposure techniques in 1994. However, electron beam and ion beam exposure techniques are not widely applied because of their high costs and high demands on the equipment.

2.4 Laser engineering techniques

The early laser engineering technique is UV light poling, which uses the strong absorption of UV laser radiation to heat up crystals locally to high temperatures. At the focus point, the coercive field of the crystal drops significantly, thus causing local domain inversion under extreme temperature gradient conditions [61–63]. UV light poling is no longer dependent on photolithography and high voltage equipment, which provides process flexibility and accuracy [61,64]. However, the domain structures can only be realized in the very shallow surface region of the crystal (usually at a depth of a few hundred nanometers), and it is easy to cause crystal surface damage. In addition, light-mediated methods for ferroelectric domain engineering, including light-assisted poling and UV laser-induced inhibition of poling, have been developed (see ref. [65] for an overview). In 2013, Thomas et al. [66] used ultrashort pulses to reduce the nonlinear coefficients of a x-cut $LiNbO_3$ crystal periodically and 1D and 2D QPM structures were obtained.

Until recently, laser writing technology was applied to direct writing of 3D domain structures in ferroelectric crystals. In 2018, Wei et al. [12] realized fabrication of the first 3D periodic domain structures in $LiNbO_3$ crystal. Figure 3(b) shows a typical setup of femtosecond laser direct writing system. The principle is to selectively erase the nonlinear coefficients $\chi^{(2)}$ inside the $LiNbO_3$ crystal. Meanwhile, Xu et al. [13] used femtosecond laser writing technique to demonstrate a 3D periodically poled $Ba_{0.77}Ca_{0.23}TiO_3$ (BCT) crystal, which is based on ferroelectric domain inversion. The realization of true 3D domain structures has always been a major challenge in the past twenty years. The experimental demonstrations [12,13] pave a way for studying new phenomena and to control nonlinear interactions in ways that were not accessible before.

3 Applications of 1D PPLN crystal

3.1 Laser frequency conversion

The reliable solid-state laser sources that are currently available cover the wavelength range from 630 to 2000 nm. However, the wavelengths that are required in the display, color printing, medical, and biological fields are often outside this range, as in the case of the demand for blue and green laser sources. The PPLN crystal based on QPM can perform frequency conversion to obtain an efficient solid-state laser source that covers the visible to UV range.

Early research on QPM-based solid-state lasers has focused on the generations of red (R), green (G), blue (B), and UV lasers. A red laser source can be obtained directly from infrared light via SHG or SFG configuration. Thompson et al. [67] obtained a 780 nm laser that was multiplied from 1560 nm to achieve a red laser with a continuous wave (CW) output of 900 mW. Chiow et al. [68] obtained a 43 W quasi-continuous red laser output with total efficiency of 66% via single-pass frequency doubling at 1560 nm. Hart et al. [69]

and Boullet et al. [70] obtained a red laser output at 630 nm using SFG of the 1060 and 1550 nm outputs from an Er^{3+}/Yb^{3+}-co-doped fiber laser. In addition, Bosenberg et al. [71] reported the use of PPLN with two periodic gratings in series to achieve a 2.5 W 629 nm red laser based on a two-step OPO and SFG process.

The common way to achieve a green laser output is through SHG. In 1997, Miller et al. [72] obtained a green CW light output of 2.7 W at 532 nm from a Nd:YAG laser using frequency doubling in PPLN; the conversion efficiency reached 42%. To provide further improvement of the efficiency, Ricciardi et al. [73] placed the PPLN crystal into a resonant cavity to achieve a conversion efficiency of up to 76% for their 6.1 W green light output.

Blue laser generation can be achieved by frequency doubling or tripling of near-infrared light. In first-order QPM materials, the challenge lies in the fabrication of small periodic domain structures (typically with periods of less than 5 μm). Pruneri et al. [74] prepared a PPLN crystal with a domain period of 4.6 μm and achieved 49 mW CW output of a 473 nm blue laser. The conversion efficiency was 4.6%. Batchko et al. [75] reported a 60 mW, 465 nm blue laser output by use of a backswitch-poled PPLN with a 4 μm period. Xu et al. [76] obtained a blue light output with a 20 nm tuning range using a 532 nm green-pumped OPO cascaded with an SHG or SFG process.

The 589 nm yellow laser has a wide range of potential uses in medical, communications, and display applications. There are two main QPM ways to produce a yellow laser. The first is based on frequency mixing of the two emission lines of Nd:YAG laser at 1064 and 1319 nm. In this method, $LiNbO_3$ [77], PPLN [78], periodically poled stoichiometric $LiTaO_3$ (PPSLT) [79] or periodically poled KTP (PPKTP) [80] crystals can be used and laser outputs of up to 16 W were obtained experimentally. The second approach is to use MgO:PPLN crystal to obtain a 589 nm narrow-linewidth CW laser output of up to 3 W by frequency doubling of a 1179 nm Raman laser [81]. $LiNbO_3$ [82,83], $LiTaO_3$ [84–87], and KTP [88–90] crystals can also be periodically poled to produce UV light. However, their inherent band edges at approximately 300 nm mean that the generated nonlinear waves cannot be moved to shorter wavelengths.

In addition, the generation of multi-wavelength solid-state lasers such as RGB three-elementary-color lasers has also attracted widespread attentions. Yamamoto et al. [91] used 1.3 and 0.86 μm laser diodes (LDs) as fundamental sources and generated 0.65 and 0.43 μm lights through SHG and 0.52 μm light through SFG in a proton exchange MgO:-$LiNbO_3$ waveguide. Cantelar et al. [92] produced a Zn-diffused Er^{3+}/Yb^{3+}-co-doped aperiodically poled $LiNbO_3$ channel waveguide to achieve a wideband-adjustable RGB laser output. Capmany achieved a RGB laser via use of a Nd^{3+}-doped PPLN crystal that was pumped using a 1084 nm/1372 nm dual-wavelength source [93].

In 1990, Feng et al. [94] proposed multiple-QPM theory, which can satisfy the phase matching conditions of multiple nonlinear processes simultaneously. In 1997, Zhu et al. [95] experimentally demonstrated cascaded THG from a single piece of quasi-periodic optical superlattice with Fibonacci sequence as shown in Figure 4(a), where the THG efficiency reached 23% (Figure 4(b)). In 2008, Hu et al. [96] used a 1064 nm/1319 nm working wavelength intermittent oscillating dual-wavelength Nd:YAG laser to achieve 1 W quasi-white-light output using a cascaded PPLT crystal; the photographic and schematic setup for quasi-white-light generation is shown in Figure 5(a) and (b). By changing the crystal temperature, the output RGB laser power ratio can be changed, allowing for the adjustment of the quasi-white-light color temperature. Figure 5(c) shows the relationship curve between RGB laser power and temperature. Another method

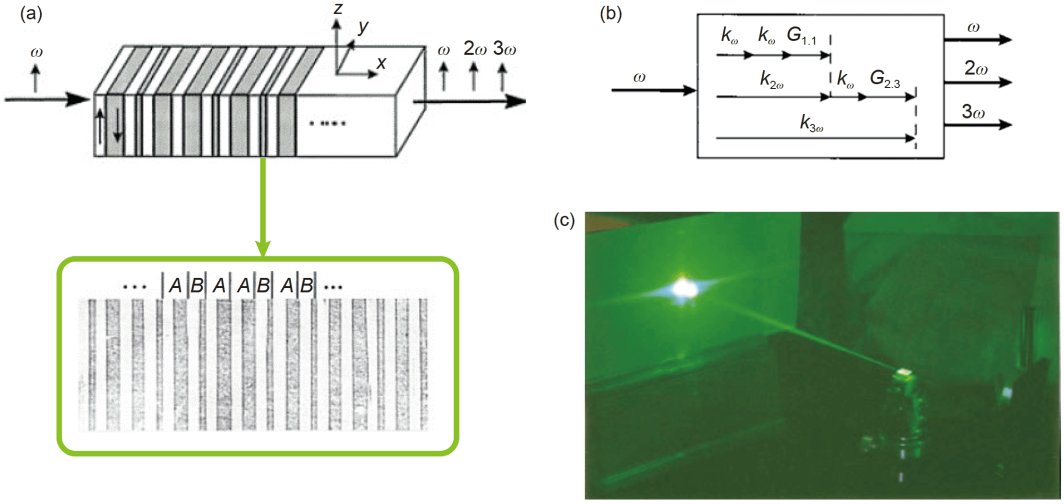

Figure 4 (Color online) (a) Quasi-periodic poled structure with a Fibonacci sequence; (b) QPM SHG and THG processes; (c) photograph of experimental test. Adapted with permission from ref. [95].

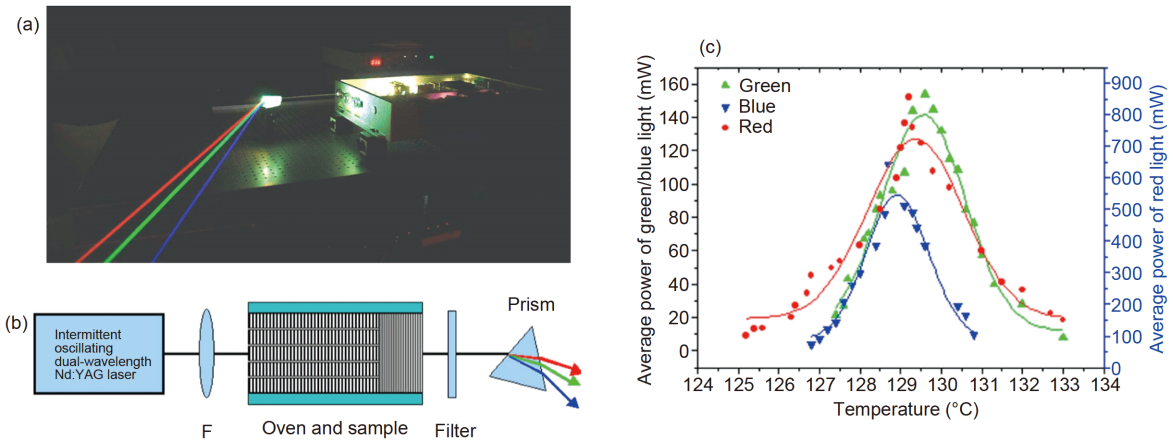

Figure 5 (Color online) (a) Photograph of the RGB quasi-white-light laser; (b) schematic setup for quasi-white-light generation; (c) temperature curves of the measured RGB lasers. Adapted with permission from ref. [96].

for RGB laser output implementation is based on frequency down-conversion and cascaded multiple frequency-upconversion processes. In 2001, Liu et al. [97] used a $LiTaO_3$ crystal with two periodic structures arranged in tandem to obtain an RGB laser output. The incident 532 nm green light was converted into 631 nm red light by frequency down-conversion. The 460 nm blue light was generated from the remaining green light and the mid-infrared (IR) idler of the former parametric process. Xu et al. [98] and Zhao et al. [99] demonstrated a noncollinear RGB laser source based on a 2D optical superlattice. The RGB laser light generated by the noncollinear reciprocal vectors was separated automatically without any requirement for optical splitting elements. Furthermore, PPLN crystals with 2D domain structures have also been employed for simultaneous laser Q-switching and optical parametric oscillation [100].

Following the development of QPM technology, new light sources have broadened the available spectral range from UV to mid-IR. QPM all-solid-state laser technology is now widely used in the modern laser industry.

3.2 Quantum sources

QPM technology has opened up a new path for quantum optics research [101]. Entangled two-photon sources are significant elements for testing of Bell inequality [102,103], quantum information [104], ghost imaging [105,106] and high-precision measurement applications [107]. Using spontaneous parametric down-conversion (SPDC), biphotons can be generated from second-order nonlinear crystals with entanglements in energy-time [108], polarization [109], and spatial modes [110]. Additionally, heralded single-photon sources [111] and multi-photon entanglement [112] can be generated by SPDC for quantum computing and quantum network applications. In previous experiments, type-Ⅱ noncollinear BPM in a nonlinear crystal was used to obtain polarization-entangled photons, with only a small portion of the emitted photons being collected [109]. To enhance the efficiency of these polarization-entangled photons [113], QPM in PPLN or PPKTP crystals is used to realize collinear phase matching, which can be applied in the cavity configuration to obtain high-brightness narrowband outputs [114,115]. Such configuration is also the main approach for the generation of high-quality squeezed state, which has widespread applications in quantum sensing and tracking [116–118]. Periodically poled crystals were used to produce sources at telecommunication wavelengths for squeezed state generation [119], optical parametric amplification [120], quantum teleportation [121], quantum key distribution [122], and quantum memory [114,123].

In addition, dual-periodically poled crystals are designed to yield polarization-entangled photon pairs, where two types of collinear reciprocal vectors take part in the SPDC process [124–126]. In 2011, Gong et al. [124] offered a scheme for the generation of counter-propagating polarization-entangled photon states from a dual-periodically poled crystal. Ueno et al. [125] demonstrated a scheme for generating polarization-entangled photon pairs with type-Ⅱ QPM-SPDC having two poled domain periods. Furthermore, aperiodically poled nonlinear crystals also supply multiple reciprocal vectors to satisfy multiple SPDC processes concurrently, leading to generation of broadband biphotons [127,128], which are promising for applications in clock synchronization [129], quantum metrology [130] and quantum optical coherence tomography [131]. In 2008, Nasr et al. [128] generated ultra-broadband biphotons (300 nm bandwidth) via chirped QPM optical parametric down-conversion in PPSLT crystal.

For high-performance quantum information processing, tremendous efforts have been made in integrated photonic circuits [132–135]. In 2014, Jin et al. [132] realized generation and manipulation of entangled photons over the telecommunication band on integrated $LiNbO_3$ waveguide

circuits. Using an annealed proton exchange process, waveguides were integrated on the PPLN, thus enabling both propagation and interference. Visibility of 92.9%±0.9% was obtained in Hong-Ou-Mandel interference and ~1.4×10^7 pairs nm^{-1} mW^{-1} photon flux was achieved. The experimental schematics are shown in Figure 6. Krapick et al. [134] abtained time-correlated photon triplets via a pulsed cascaded parametric down-conversion process in an integrated $LiNbO_3$ chip. In 2018, Atzeni et al. [135] obtained polarization entanglement photons using a chip composed of hybrid materials with femtosecond-laser-written technology, for which the visibility exceeded 92%.

4 Applications of 2D PPLN crystal

4.1 Nonlinear beam shaping

One important application of 2D PPLN crystal is nonlinear beam shaping based on various QPM configurations. In refs. [136–138], nonlinear beam shaping has been well overviewed. Here, we briefly introduce several classic examples. Xu et al. [139] proposed a scattering-assisted QPM mechanism for nonlinear shaping of conical beams. Figure 7(b) illustrates the reciprocal vector of the hexagonally poled PPLT structure shown in Figure 7(a). When the fundamental wavelength is gradually detuned from the traditional phase matching point toward a longer wavelength, the far field SH pattern gradually changes from a point into a ring, and the radius of the ring expands continuously (Figure 7(c) and (d)). This phenomenon is caused by a new mechanism in which the fundamental scattered light participates in the phase matching process (Figure 7(e) and (f)). This novel QPM mechanism offers new possibilities for engineering of nonlinear interactions, and it can also be used to disclose the internal information of the PPLN structure. Recently, such scattering-assisted configuration has been extended to conical THG [140].

Allen et al. [141] proposed that the vortex beam's spiral wave-front is the root of orbital angular momentum (OAM) in 1992. Generally, the vortex beam including Laguerre-Gaussian (LG) beam and Bessel beam has a phase singularity, which forms a ring-shaped profile with a dark center. The spiral wave-front can be described using $\exp(il\varphi)$, where l is the topological charge. These novel characteristics have been applied in optical tweezers [142–145], optical communications [146,147], rotation measurement [148] and quantum information processing [149]. It has been extensively studied to use spatial light modulators, fork gratings, meta-surface devices, and cylindrical lenses to produce vortex beams. 2D PPLN crystals provide a compact way to produce vortex beams at new frequencies, which have attracted increasing research interests. Shapira et al. [150] used holographic theory to design the binary modulation function of the nonlinear coefficient to realize two-dimensional nonlinear beam shaping, which was given as follows [151]:

$$d_{\mathrm{NLO}}(x,y) = d_{ij}\mathrm{sign}\left\{\cos[2\pi f_{\mathrm{carrier}}x-\varphi(x,y)]-\cos[\pi q(x,y)]\right\}, \quad (1)$$

where d_{ij} is the element of quadratic susceptibility $\chi^{(2)}$ tensor, $\varphi(x,y)$ is the phase of the target light field after Fourier transformation, the amplitude $A(x,y)$ is given by $\sin[\pi q(x,y)] = A(x,y)$, f_{carrier} is the carrier frequency that determines the diffraction angle. The first-order SH diffraction is the desired light field. The fundamental beam propagates along the z-axis. Because the electrical poling technique is limited to the x-y plane, only the transverse phase matching condition can be satisfied in 2D nonlinear beam shaping process. Figure 8(a) shows a typical experimental scheme, in which the target SH light field is generated by the nonlinear Raman-Nath process on first-order diffraction. The nonlinear crystal is irradiated with a Gaussian

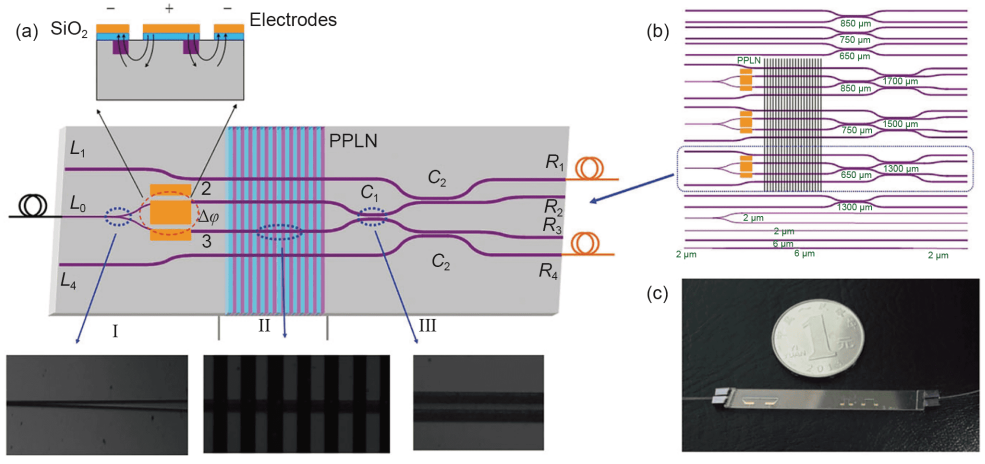

Figure 6 (Color online) (a) Schematics of integrated $LiNbO_3$ waveguide circuits; (b) detailed structure of the chip; (c) photograph of the chip. Adapted with permission from ref. [132].

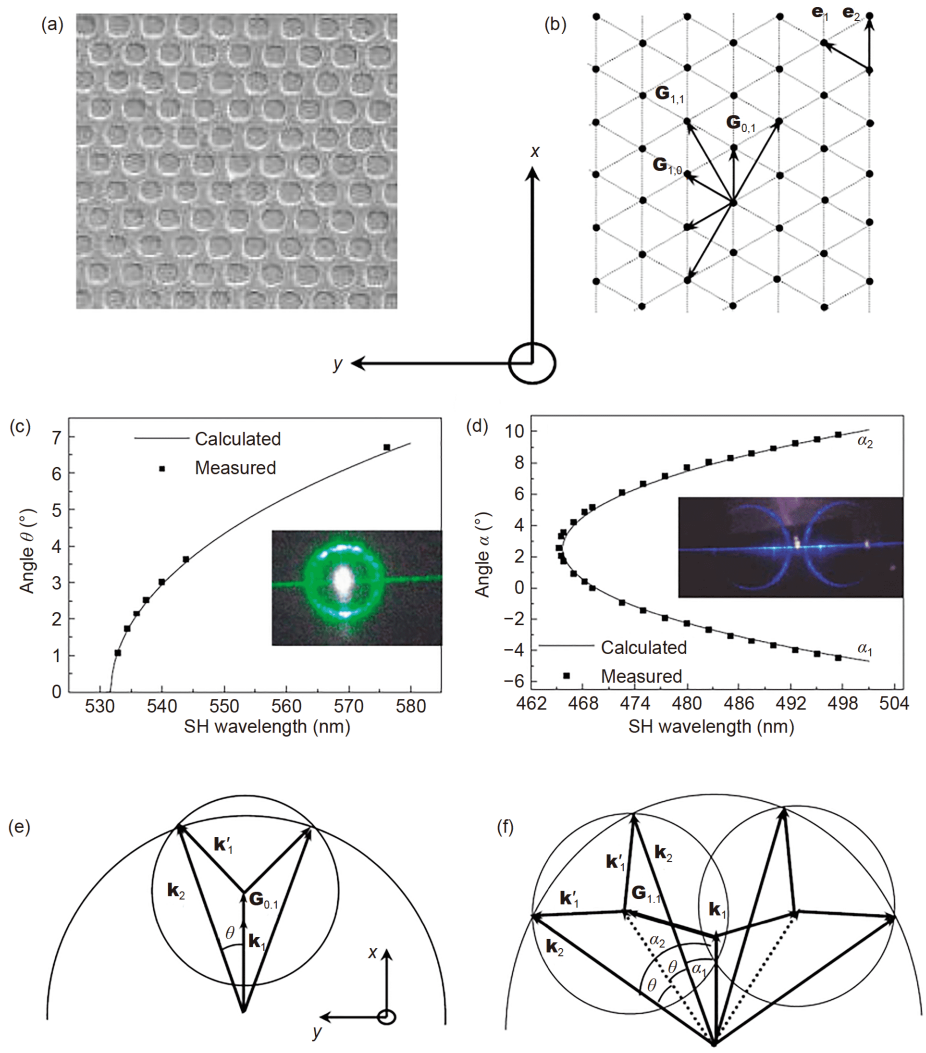

Figure 7 (Color online) (a) Structure of hexagonal domain structure; (b) the reciprocal vectors; (c), (d) the measured patterns and angles as a function of SH wavelength for a single ring and a pair of rings, respectively; (e), (f) the phase matching mechanisms. Adapted with permission from ref. [139].

mode fundamental wave, and an SH vortex beam and an SH Hermitian-Gaussian (HG) beam are generated, as shown in Figure 8(b) and (c), respectively.

In 2012, Bloch et al. [152] studied nonlinear vortex beam generation in a fork-grating poled $LiTaO_3$ crystal that carried a topological charge l_c. As shown in Figure 9(a), the Gaussian mode fundamental wave passes through the nonlinear crystal and an SH vortex beam with a topological charge of $\pm ml_c$ can be obtained at the $\pm m$ orders of diffraction, respectively. When fundamental wave carries a non-zero OAM as shown in Figure 9(b), the law of OAM conversion during frequency doubling satisfies [153]:

$$l_{2\omega,m} = 2 \cdot l_{\omega} + m \cdot l_c, \tag{2}$$

where $l_{2\omega}$ and l_{ω} are the topological charges of the SH and fundamental wave, respectively.

Diffraction is a general phenomenon in light propagation, but one type of beam can maintain non-spreading properties over a certain distance, which is called a diffraction-free beam. The Airy beam is a typical diffraction-free beam, which can be described using the Airy function [154]. The Airy beam has self-healing and self-acceleration features. In linear experiments, Gaussian beams are modulated using a cubic phase and are then Fourier transformed to obtain Airy beams [155]. In PPLN crystals, the wave front of the second harmonic can also be controlled continuously by properly designing the domain structure. In 2009, Ellenbogen et al. [156] designed a 2D nonlinear modulation pattern shaped like an "S" to realize nonlinear generation and manipulation of Airy beams. The second-order nonlinear coefficient modulation function is given as follows:

$$\chi^{(2)}(x,y) = d_{ij}\mathrm{sign}\left[\cos\left(2\pi f_x x + f_c y^3\right)\right]. \tag{3}$$

The generated SH wave is then subjected to a lens Fourier transform, allowing a 1D SH Airy beam to be obtained at the back focal plane. Interestingly, dynamic control of the SH

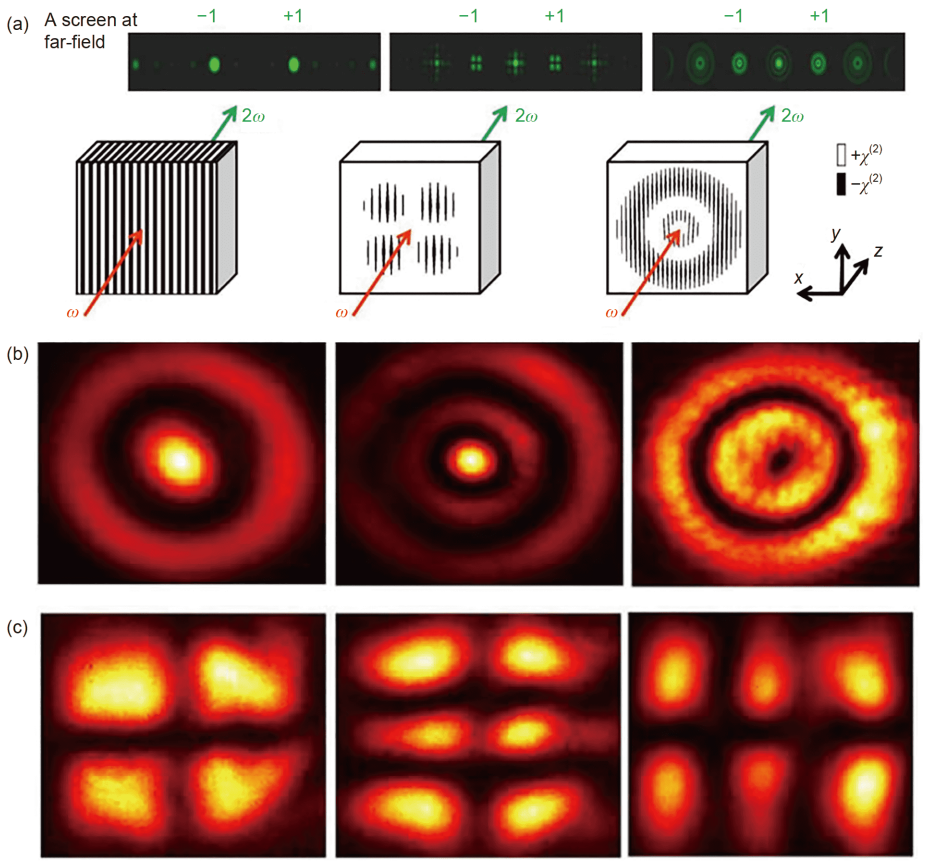

Figure 8 (Color online) (a) Schematic of 2D nonlinear beam shaping process; (b) experimentally generated SH LG beam pattern; (c) experimentally generated SHG beam pattern. Adapted with permission from ref. [150].

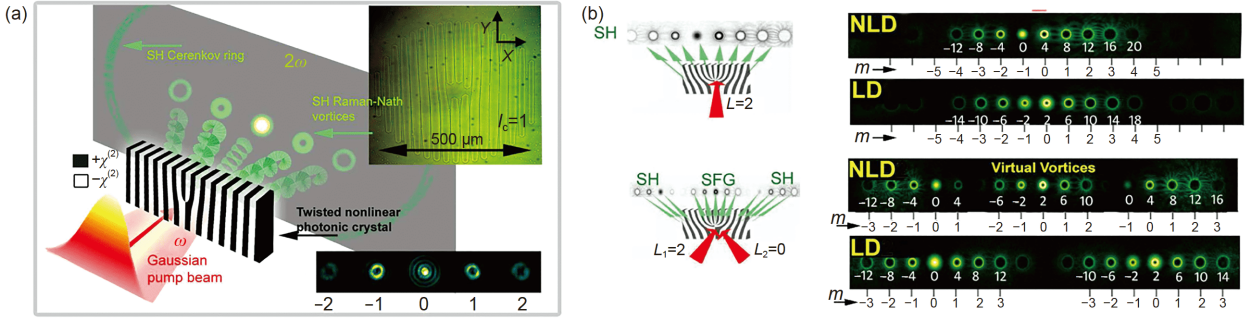

Figure 9 (Color online) (a) Various SH vortex beams are generated through nonlinear Raman-Nath diffraction; (b) OAM of the diffracted vortex beams are conserved in the linear and nonlinear processes. Adapted with permission from ref. [152].

Airy beam can be realized by adjusting either the temperature or the fundamental wavelength.

4.2 Quantum light sources in 2D PPLN crystal

In SPDC, a 1D PPLN crystal can provide collinear RLVs for generation of two-photon states. The collinear and non-collinear RLVs in 2D PPLN crystals provide a potential way to manipulate the spatial mode of a two-photon state such as spatial entanglement and path-entangled states in infinite dimensional Hilbert space. Spatial mode entanglement can be used to increase the efficiency of quantum communications [157] and quantum imaging [158]. Multi-path entanglement also plays an important role in quantum lithography [159] and quantum precision measurement [107] applications. In 2004, Torres et al. [157] proposed QPM engineering for the spatial control of entangled photons. In 2008, Yu et al. [160] fabricated a multi-stripe periodically poled structure and modulated the spatial correlation of the two-photon state using SPDC (Figure 10). The far-field diffraction interference revealed the transverse modulation of the domain patterns as shown in Figure 11. In 2011, Leng

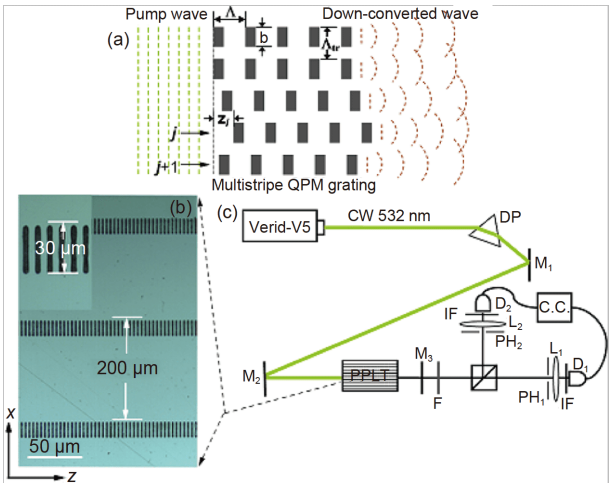

Figure 10 (Color online) (a) Schematic of the multistripe PPLT crystal; (b) the structure image; (c) experimental setup. Adapted with permission from ref. [160].

et al. [161] steered a spatially entangled two-photon state in a PPLT crystal with a parabolic phase profile. When changing the position of the pump light, the role of PPLT crystal is to focus or dual-focus the entangled photon pairs. The quantum Talbot effect was also observed from a domain-engineered nonlinear crystals [162].

The path-entangled state can be transformed into a hyper-entangled state [163,164] and a cluster state [165]. However, the general ways to obtain the path-entangled state are not integrated and are not sufficiently stable [166]. The 2D PPLN crystal supplies a good solution. When the pump light passes through a 2D PPLN crystal, multiple RLVs take part in SPDC for the generation of the multipath-entangled state. In 2013, Megidish et al. [167] produced a beam-like path-entangled state in a rectangular lattice domain-engineered structure, in which two entangled photons propagated collinearly along either one of two paths. Additionally, Jin et al. [168] fabricated a hexagonally poled PPLT crystal to obtain a beam-like path-entangled state and a heralded single-photon path-entangled state by modifying the crystal temperature (Figure 12).

Furthermore, many schemes with 2D PPLN crystals were proposed for more complex quantum engineering applications [169–173], e.g., the polarization-entangled state [170], the multipath Dicke state [169], and manipulation of the OAM of entangled two-photon states [171,172]. These efforts paved a desirable way for miniaturization of quantum technologies.

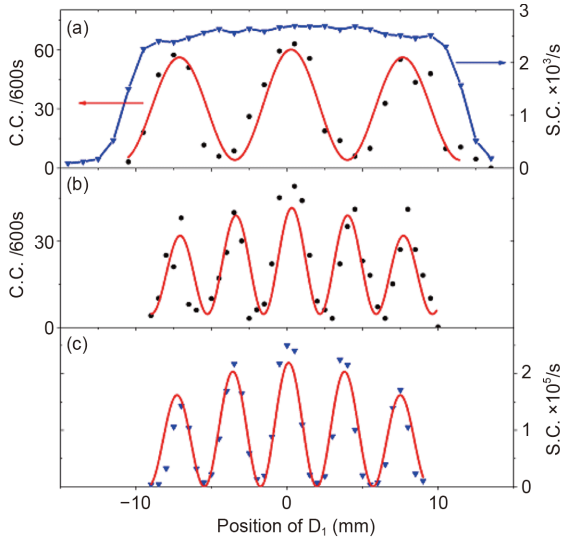

Figure 11 (Color online) Coincidence counts and single counts versus the position of detector D_1. (a) Detector D_2 was fixed; (b) both D_1 and D_2 were scanned; (c) single counts measured when the sample mask was illuminated by the pump light. The solid red curves denote theoretical fitting. Adapted with permission from ref. [160].

5 Nonlinear optical imaging of domain structures

Techniques for observation of the domain structure in periodically-poled crystals are generally divided into electron microscopy and optical imaging technology approaches. Electron microscopy techniques mainly include SEM [174,175] and transmission electron microscopy (TEM) [176]. Use of linear optical imaging requires the crystal itself to have a refractive index change, which is generally difficult for the domain structure in a periodically-poled crystal with its uniform refractive index. Therefore, it is often necessary to corrode and destroy the crystal to change the relevant properties near the domain wall [177]. Nonlinear optical imaging takes advantage of the nonlinear effects from the domain structure to detect nonlinear signals directly and thus obtain the domain structure images. SHG is one of the most widely used methods.

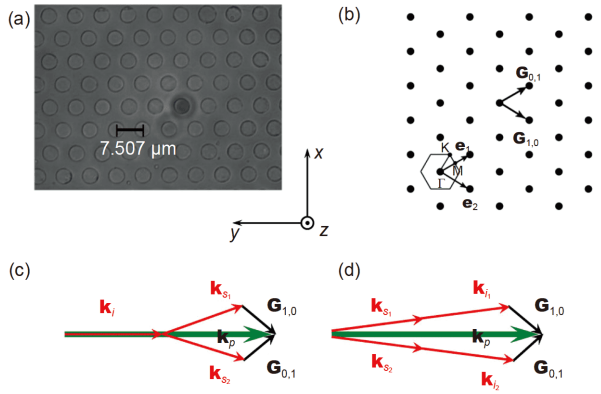

Figure 12 (Color online) (a) Image of the hexagonally poled $LiNbO_3$ crystal; (b) the reciprocal vectors; (c), (d) phase matching configurations for single-photon and two-photon path entanglements, respectively. Adapted with permission from ref. [168].

The nonlinear Talbot self-imaging effect is an interesting phenomenon and has been used in the nonlinear domain imaging field. In 1836, Talbot [178] discovered for the first time that the diffraction intensity distribution from a periodically structured object is similar to the structure itself at a specific position; this lensless self-imaging effect is called the Talbot effect. Zhang et al. [179] extended the Talbot effect to the nonlinear optics field and reported the first experimental observation of nonlinear Talbot effect in 2010. For an artificially periodically poled nonlinear crystal, the SH generated by the crystal is also a periodically distributed light field. According to the Talbot effect, SH self-imaging should be observed at a specific position relative to the crystal, and the light intensity of the SH indicates the distribution of the domain structure. As shown in Figure 13(a), by adjusting the objective lens position to obtain the light field distributions at the different imaging planes, the experiments test the 1D and 2D domain structures. For 1D case (Figure 13(b)), the SH Talbot distance is $z_T=4a^2/\lambda_p$, where a is the structure period and λ_p is the fundamental wavelength. The SH images obtained on the first and third Talbot planes are shown in Figure 13(c) and (d), respectively, where the SH field reproduces the domain structure very well. For the 2D hexagonal domain structure (Figure 13(e)), the SH Talbot distance is $z_T=3a^2/\lambda_p$. Figure 13(f) and (g) shows the first and third Talbot plane images, respectively, which is consistent with the domain structure distribution.

Cerenkov SHG is generally used for nonperiodic domain structure imaging; the fundamental wave is focused on the structure, the SH signal is detected, and the domain structure distribution imaging is performed by point-by-point scanning [26]. This method is capable to observe 3D domain structures [12,13,180,181]. Recently, Lu et al. [182] proposed a novel imaging method that used the nearly diffraction-free SH dark fringes generated at the domain wall to image the irregularly distributed domain structure without scanning. As shown in Figure 14(a), the domain polarization directions on the two sides of the wall are opposite, which indicates a π phase difference in the SH waves, and the interference then forms a dark line. After theoretical derivation, the relationship between the line width and the propagation distance of the dark line is found to be $w \propto \sqrt{\lambda z}$ (Figure 14(a)). Figure 14(b) shows the experimental results obtained from a disordered domain structure.

6 Applications of 3D domain structures

6.1 3D nonlinear beam shaping

In 2018, Wei et al. [12] and Xu et al. [13] used femtosecond laser direct writing technology to realize preparation of 3D domain structures based on different processing mechanisms. This was the first time that 3D nonlinear coefficient modulation was experimentally realized. The 3D domain structure can provide abundant reciprocal vectors in 3D space to satisfy the full QPM conditions in the nonlinear

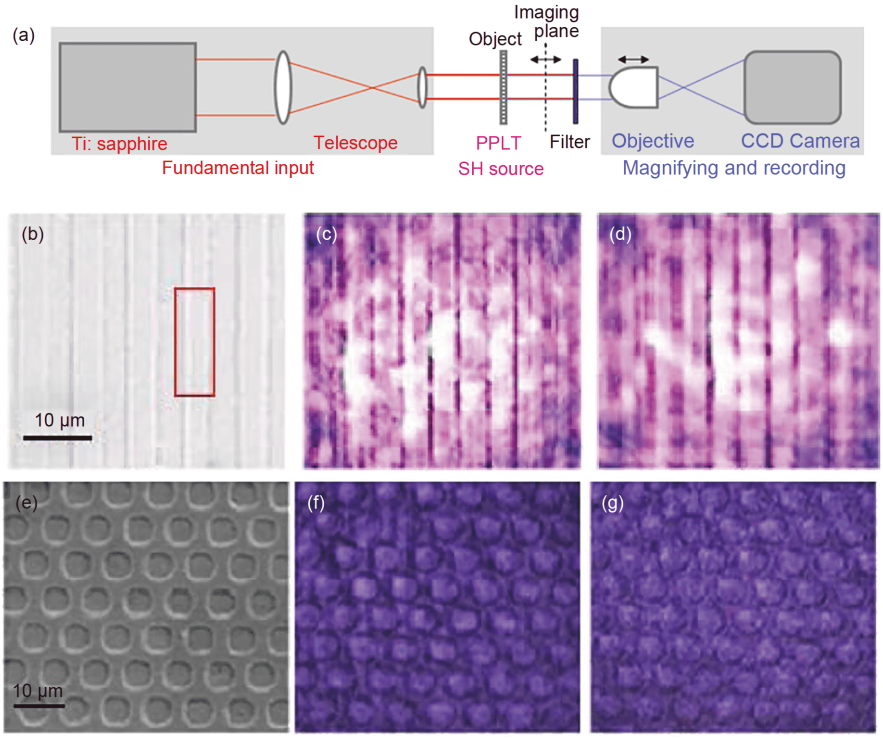

Figure 13 (Color online) (a) Schematic of experimental setup; (b), (e) 1D and 2D domain structure; (c), (f) SH self-images at the first Talbot plane; (d), (g) SH self-images at the third Talbot plane. Adapted with permission from ref. [179].

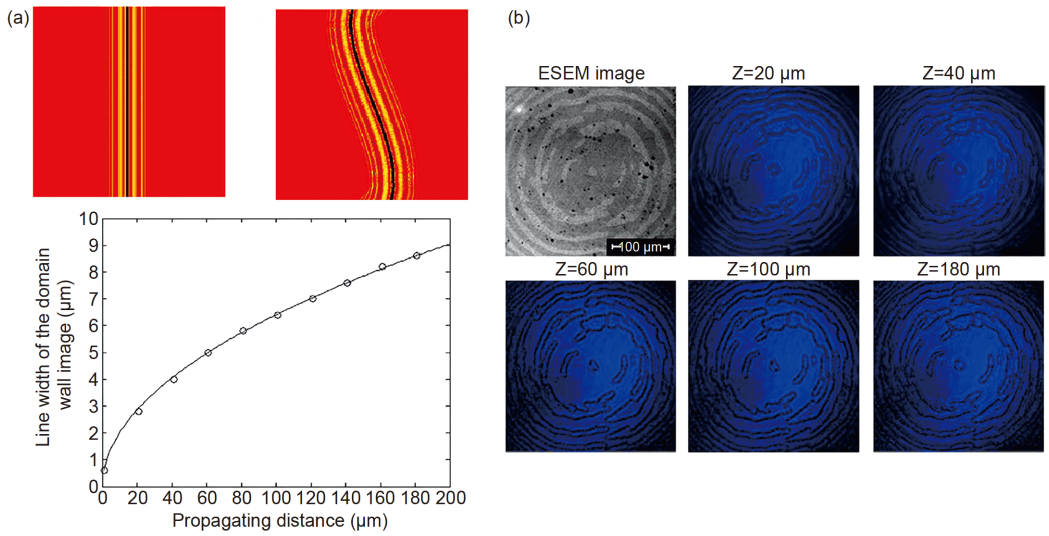

Figure 14 (Color online) (a) Simulated SH images and line width for single domain wall; (b) experimental SH images acquired at different distances from the crystal. Adapted with permission from ref. [182].

process and realize efficient modulation of the frequency, amplitude and phase of the light. It thus shows exciting potential for integrated control of nonlinear waves. Take nonlinear beam shaping as an example. In comparison to 2D nonlinear beam shaping, 3D case can achieve higher nonlinear beam shaping efficiency and multiple beam wavefront processing.

In 2019, Wei et al. [180] experimentally realized efficient nonlinear beam shaping in 3D-engineered $LiNbO_3$ crystal. 2D nonlinear beam shaping is generally realized via nonlinear Raman-Nath process, in which the conversion efficiency is limited by the longitudinal phase mismatch. In 3D case, the transvers and longitudinal phase matching conditions can be satisfied simultaneously to enhance the nonlinear beam shaping efficiency. Based on binary holographic theory and the QPM conditions, they designed the nonlinear coefficient modulation function of the 3D structure as follows:

$$f(x,y,z) = T\left\{\cos\left[G_x x - \arg(E_{2\omega})\right] - \cos\left[\sin^{-1}\mathrm{amp}(E_{2\omega})\right]\right\} \times T\left[\cos\left(G_y y\right)\right]. \quad (4)$$

In eq. (4), $E_{2\omega}$ is the desired light field. As shown in Figure 15, the 3D nonlinear structure provides an additional reciprocal vector G_y along the propagation direction so that the QPM condition is completely satisfied and the SH beam shaping efficiency is enhanced. Besides, the phase matching condition can be altered by varying the fundamental wavelength and selecting a specific diffraction order to be brightened.

Liu et al. [181] used a tightly focused femtosecond laser to form a thermoelectric field at the focal point in a crystal, thus inducing locally poled domain structure in BCT crystals. In the experiment, they fabricate multilayer 2D structures at different depths. As shown in Figure 16(a) and (b), when compared with the 2D nonlinear beam shaping, the additional dimension in the depth direction allows multiple beam wavefront generations. Figure 16(c)–(e) shows schematics of three structures. The fork gratings with different angles in Figure 16(c) generated far-field SH vortex beams at ±1st order diffraction in three directions as shown in Figure 16(f); the structure in Figure 16(d) includes a concentric ring, a common grating and a fork grating at different depths, and the SH distribution is the superposition of the far-field diffraction patterns of these three structures as shown in Figure 16(g).

6.2 Potential applications of 3D domain structures

Besides 3D nonlinear beam shaping, 3D domain structures have potential applications in nonlinear multiplexing, cascaded nonlinear optical processes, THz sources, and quantum optics [183]. In comparison to 1D and 2D structures, 3D domain structures naturally have higher information capacities, which can be effectively utilized in information coding, high-quality nonlinear holography, and so on. The 3D RLVs make it possible to control multiple nonlinear optical processes simultaneously in 3D space, which is not accessible before. In quantum state engineering, a 3D structure provides an integrated platform for steering of the spatial degree of freedom of the entangled two-photon states. For example, 3D domain structures can increase the dimensionality and quantity of path-entangled states simultaneously. The experimental demonstrations are ongoing.

7 Conclusion

In 1980, the first PPLN crystal was fabricated by crystal

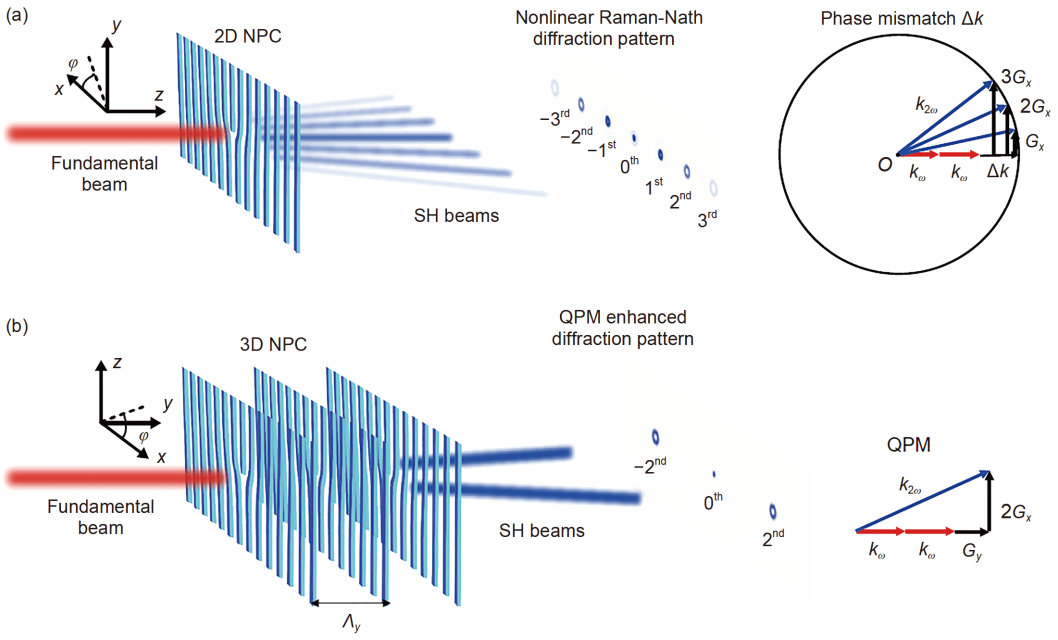

Figure 15 (Color online) Schematics of (a) nonlinear Raman-Nath diffraction in 2D domain structure and (b) QPM enhanced diffraction in 3D domain structure. Adapted with permission from ref. [180].

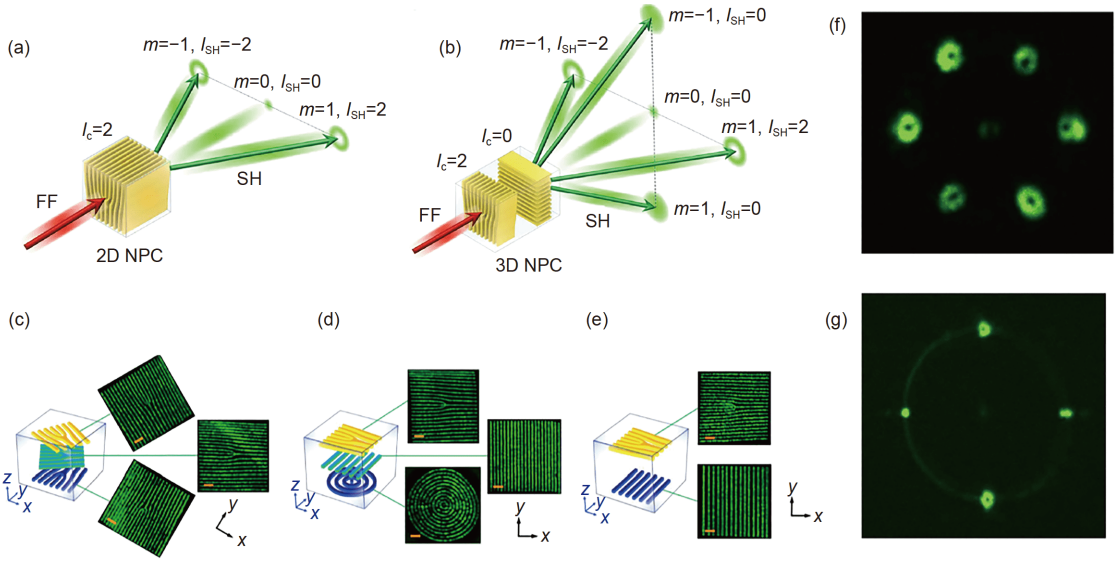

Figure 16 (Color online) (a), (b) Schematics of SH diffraction from 2D and 3D domain structures, respectively; (c)–(e) schematics of three types of domain structures; (f) far-field SH diffraction from the structure in (c); (g) far-field SH diffraction from the structure in (d). Adapted with permission from ref. [181].

growth method, which opens the door to investigate QPM in experiment. 40 years later, PPLN crystal has been extended from 1D to 2D and 3D, and its applications have been developed from frequency conversion to nonlinear beam shaping, quantum entangled source, and integrated photonic circuits. PPLN crystal is still an active topic and the related researches are prospective.

This work was supported by the National Key R&D Program of China (Grant Nos. 2017YFA0303703 and 2016YFA0302500), the National Natural Science Foundation of China (Grant Nos. 91950206, 11874213 and 11674171), and the Fundamental Research Funds for the Central Universities (Grant Nos. 14380105 and 1480605201).

1 Maiman T H, Hoskins R H, D'Haenens I J, et al. Stimulated optical emission in fluorescent solids. II. Spectroscopy and stimulated emission in ruby. Phys Rev, 1961, 123: 1151–1157
2 Franken P A, Hill A E, Peters C W, et al. Generation of optical harmonics. Phys Rev Lett, 1961, 7: 118–119
3 Kleinman D A. Theory of second harmonic generation of light. Phys Rev, 1962, 128: 1761–1775
4 Armstrong J A, Bloembergen N, Ducuing J, et al. Interactions be-

tween light waves in a nonlinear dielectric. Phys Rev, 1962, 127: 1918–1939
5 Ming N B, Hong J F, Feng D. The growth striations and ferroelectric domain structures in Czochralski-grown $LiNbO_3$ single crystals. J Mater Sci, 1982, 17: 1663–1670
6 Feng D, Ming N, Hong J, et al. Enhancement of second-harmonic generation in $LiNbO_3$ crystals with periodic laminar ferroelectric domains. Appl Phys Lett, 1980, 37: 607–609
7 Yamada M, Nada N, Saitoh M, et al. First-order quasi-phase matched $LiNbO_3$ waveguide periodically poled by applying an external field for efficient blue second-harmonic generation. Appl Phys Lett, 1993, 62: 435–436
8 Lu Y, Lu Y, Xue C, et al. Growth of Nd^{3+}-doped $LiNbO_3$ optical superlattice crystals and its potential applications in self-frequency doubling. Appl Phys Lett, 1996, 68: 1467–1469
9 Zheng J, Lu Y, Luo G, et al. Visible dual-wavelength light generation in optical superlattice Er:$LiNbO_3$ through upconversion and quasi-phase-matched frequency doubling. Appl Phys Lett, 1998, 72: 1808–1810
10 Rosenman G, Urenski P, Agronin A, et al. Submicron ferroelectric domain structures tailored by high-voltage scanning probe microscopy. Appl Phys Lett, 2003, 82: 103–105
11 Hsu W, Gupta M C. Domain inversion in $LiTaO_3$ by electron beam. Appl Phys Lett, 1992, 60: 1–3
12 Wei D, Wang C, Wang H, et al. Experimental demonstration of a three-dimensional lithium niobate nonlinear photonic crystal. Nat Photon, 2018, 12: 596–600
13 Xu T, Switkowski K, Chen X, et al. Three-dimensional nonlinear photonic crystal in ferroelectric barium calcium titanate. Nat Photon, 2018, 12: 591–595
14 Saltiel S M, Sheng Y, Voloch-Bloch N, et al. Cerenkov-type second-harmonic generation in two-dimensional nonlinear photonic structures. IEEE J Quantum Electron, 2009, 45: 1465–1472
15 Zhang Y, Gao Z D, Qi Z, et al. Nonlinear Čerenkov radiation in nonlinear photonic crystal waveguides. Phys Rev Lett, 2008, 100: 163904
16 Sheng Y, Saltiel S M, Krolikowski W, et al. Čerenkov-type second-harmonic generation with fundamental beams of different polarizations. Opt Lett, 2010, 35: 1317–1319
17 Wang W, Sheng Y, Kong Y, et al. Multiple Čerenkov second-harmonic waves in a two-dimensional nonlinear photonic structure. Opt Lett, 2010, 35: 3790–3792
18 Shutov I V, Ozheredov I A, Shumitski A V, et al. Second harmonic generation by femtosecond laser pulses in the Laue scheme. Opt Spectrosc, 2008, 105: 79–84
19 Molina P, Ramírez M O, García B J, et al. Directional dependence of the second harmonic response in two-dimensional nonlinear photonic crystals. Appl Phys Lett, 2010, 96: 261111
20 Zembrod A, Puell H, Giordmaine J A. Surface radiation from nonlinear optical polarisation. Opto-electronics, 1969, 1: 64–66
21 Kaminskii A A, Nishioka H, Ueda K, et al. Second-harmonic generation with Cherenkov-type phase matching in a bulk nonlinear $LaBGeO_5$ crystal. Quantum Electron, 1996, 26: 381–382
22 Vaičaitis V. Cherenkov-type phase matching in bulk KDP crystal. Optics Commun, 2002, 209: 485–490
23 Sheng Y, Kong Q, Roppo V, et al. Theoretical study of Čerenkov-type second-harmonic generation in periodically poled ferroelectric crystals. J Opt Soc Am B, 2012, 29: 312–318
24 Zhang Y, Wang F, Geren K, et al. Second-harmonic imaging from a modulated domain structure. Opt Lett, 2010, 35: 178–180
25 Huang X, Wei D, Wang Y, et al. Second-harmonic interference imaging of ferroelectric domains through a scanning microscope. J Phys D-Appl Phys, 2017, 50: 485105
26 Sheng Y, Best A, Butt H J, et al. Three-dimensional ferroelectric domain visualization by Čerenkov-type second harmonic generation. Opt Express, 2010, 18: 16539–16545
27 Zhang Y, Qi Z, Wang W, et al. Quasi-phase-matched Čerenkov second-harmonic generation in a hexagonally poled $LiTaO_3$ waveguide. Appl Phys Lett, 2006, 89: 171113
28 Chen C D, Zhang Y, Zhao G, et al. Experimental realization of Cerenkov up-conversions in a 2D nonlinear photonic crystal. J Phys D-Appl Phys, 2012, 45: 405101
29 Chen C, Lu J, Liu Y, et al. Cerenkov third-harmonic generation via cascaded $\chi^{(2)}$ processes in a periodic-poled $LiTaO_3$ waveguide. Opt Lett, 2011, 36: 1227–1229
30 Zhang Y, Hu X P, Zhao G, et al. Cerenkov second-harmonic arc from a hexagonally poled $LiTaO_3$ planar waveguide. J Phys D-Appl Phys, 2009, 42: 215103
31 Saltiel S M, Neshev D N, Krolikowski W, et al. Multiorder nonlinear diffraction in frequency doubling processes. Opt Lett, 2009, 34: 848–850
32 Saltiel S M, Neshev D N, Fischer R, et al. Generation of second-harmonic conical waves via nonlinear bragg diffraction. Phys Rev Lett, 2008, 100: 103902
33 Freund I. Nonlinear diffraction. Phys Rev Lett, 1968, 21: 1404–1406
34 Zhu Y Y, Hong J F, Ming N B. Growth of ferroelectric crystals from melt. Ferroelectrics, 1993, 142: 31–44
35 Chen J, Zhou Q, Hong J F, et al. Influence of growth striations on para-ferroelectric phase transitions: Mechanism of the formation of periodic laminar domains in $LiNbO_3$ and $LiTaO_3$. J Appl Phys, 1989, 66: 336–341
36 Wenshan W, Qun Z, Zhaohua G, et al. Study of $LiTaO_3$ crystals grown with a modulated structure I. Second harmonic generation in $LiTaO_3$ crystals with periodic laminar ferroelectric domains. J Cryst Growth, 1986, 79: 706–709
37 Xu H, Jiang G, Mao L, et al. High-frequency resonance in acoustic superlattice of barium sodium niobate crystals. J Appl Phys, 1992, 71: 2480–2482
38 Wenshan W, Ming Q I. Research on TGS single crystal growth with modulated structure. J Cryst Growth, 1986, 79: 758–761
39 Fejer M M, Magel G A, Jundt D H, et al. Quasi-phase-matched second harmonic generation: Tuning and tolerances. IEEE J Quantum Electron, 1992, 28: 2631–2654
40 Foulon G, Ferriol M, Brenier A, et al. Laser heated pedestal growth and optical properties of Yb^{3+}-doped $LiNbO_3$ single crystal fibers. Chem Phys Lett, 1995, 245: 555–560
41 Miyazawa S. Ferroelectric domain inversion in Ti-diffused $LiNbO_3$ optical waveguide. J Appl Phys, 1979, 50: 4599–4603
42 Zhu Y, Zhu S, Hong J, et al. Domain inversion in $LiNbO_3$ by proton exchange and quick heat treatment. Appl Phys Lett, 1994, 65: 558–560
43 Lim E J, Fejer M M, Byer R L. Second-harmonic generation of green light in periodically poled planar lithium niobate waveguide. Electron Lett, 1989, 25: 174–175
44 Lim E J, Fejer M M, Byer R L, et al. Blue light generation by frequency doubling in periodically poled lithium niobate channel waveguide. Electron Lett, 1989, 25: 731–732
45 Webjorn J, Laurell F, Arvidsson G. Blue light generated by frequency doubling of laser diode light in a lithium niobate channel waveguide. IEEE Photon Technol Lett, 1989, 1: 316–318
46 Webjorn J, Laurell F, Arvidsson G. Fabrication of periodically domain-inverted channel waveguides in lithium niobate for second harmonic generation. J Lightwave Technol, 1989, 7: 1597–1600
47 Niu Y, Lin C, Liu X, et al. Optimizing the efficiency of a periodically poled LNOI waveguide using *in situ* monitoring of the ferroelectric domains. Appl Phys Lett, 2020, 116: 101104
48 Zhu S, Zhu Y, Zhang Z, et al. $LiTaO_3$ crystal periodically poled by applying an external pulsed field. J Appl Phys, 1995, 77: 5481–5483
49 Risk W P, Lau S D. Periodic electric field poling of $KTiOPO_4$ using chemical patterning. Appl Phys Lett, 1996, 69: 3999–4001
50 Canalias C, Pasiskevicius V. Mirrorless optical parametric oscillator. Nat Photon, 2007, 1: 459–462
51 Myers L E, Eckardt R C, Fejer M M, et al. Quasi-phase-matched optical parametric oscillators in bulk periodically poled $LiNbO_3$. J

Opt Soc Am B, 1995, 12: 2102–2116
52 Batchko R G, Shur V Y, Fejer M M, et al. Backswitch poling in lithium niobate for high-fidelity domain patterning and efficient blue light generation. Appl Phys Lett, 1999, 75: 1673–1675
53 Busacca A C, Sones C L, Apostolopoulos V, et al. Surface domain engineering in congruent lithium niobate single crystals: A route to submicron periodic poling. Appl Phys Lett, 2002, 81: 4946–4948
54 Busacca A C, Sones C L, Eason R W, et al. First-order quasi-phase-matched blue light generation in surface-poled Ti:indiffused lithium niobate waveguides. Appl Phys Lett, 2004, 84: 4430–4432
55 Kuroda A, Kurimura S, Uesu Y. Domain inversion in ferroelectric MgO:$LiNbO_3$ by applying electric fields. Appl Phys Lett, 1996, 69: 1565–1567
56 Ishizuki H, Taira T. High-energy quasi-phase-matched optical parametric oscillation in a periodically poled MgO:$LiNbO_3$ device with a 5 mm×5 mm aperture. Opt Lett, 2005, 30: 2918–2920
57 Ishizuki H, Taira T. Half-joule output optical-parametric oscillation by using 10-mm-thick periodically poled Mg-doped congruent $LiNbO_3$. Opt Express, 2012, 20: 20002–20010
58 Sheng Y, Wang T, Ma B, et al. Anisotropy of domain broadening in periodically poled lithium niobate crystals. Appl Phys Lett, 2006, 88: 041121
59 Rosenman G, Garb K, Skliar A, et al. Domain broadening in quasi-phase-matched nonlinear optical devices. Appl Phys Lett, 1998, 73: 865–867
60 Mizuuchi K, Yamamoto K. Second-harmonic generation in domain-inverted grating induced by focused ion beam. OPT REV, 1994, 1: 100–102
61 Boes A, Steigerwald H, Crasto T, et al. Tailor-made domain structures on the *x*- and *y*-face of lithium niobate crystals. Appl Phys B, 2014, 115: 577–581
62 Steigerwald H, Ying Y J, Eason R W, et al. Direct writing of ferroelectric domains on the *x*- and *y*-faces of lithium niobate using a continuous wave ultraviolet laser. Appl Phys Lett, 2011, 98: 062902
63 Boes A, Crasto T, Steigerwald H, et al. Direct writing of ferroelectric domains on strontium barium niobate crystals using focused ultraviolet laser light. Appl Phys Lett, 2013, 103: 142904
64 Muir A C, Sones C L, Mailis S, et al. Direct-writing of inverted domains in lithium niobate using a continuous wave ultra violet laser. Opt Express, 2008, 16: 2336–2350
65 Ying C Y J, Muir A C, Valdivia C E, et al. Light-mediated ferroelectric domain engineering and micro-structuring of lithium niobate crystals. Laser Photon Rev, 2012, 6: 526–548
66 Thomas J, Hilbert V, Geiss R, et al. Quasi phase matching in femtosecond pulse volume structured *x*-cut lithium niobate. Laser Photonics Rev, 2013, 7: L17–L20
67 Thompson R, Tu M, Aveline D, et al. High power single frequency 780 nm laser source generated from frequency doubling of a seeded fiber amplifier in a cascade of PPLN crystals. Opt Express, 2003, 11: 1709–1713
68 Chiow S, Kovachy T, Hogan J M, et al. Generation of 43 W of quasi-continuous 780 nm laser light via high-efficiency, single-pass frequency doubling in periodically poled lithium niobate crystals. Opt Lett, 2012, 37: 3861–3863
69 Hart D L, Goldberg L, Burns W K. Red light generation by sum frequency mixing of Er/Yb fibre amplifier output in QPM $LiNbO_3$. Electron Lett, 1999, 35: 52–53
70 Boullet J, Lavoute L, Desfarges Berthelemot A, et al. Tunable red-light source by frequency mixing from dual band Er/Yb co-doped fiber laser. Opt Express, 2006, 14: 3936–3941
71 Bosenberg W R, Alexander J I, Myers L E, et al. 2.5 W, continuous wave, 629 nm solid-state laser source. In: Proceedings of the Advanced Solid State Lasers. Coeur d'Alene: Optical Society of America, 1998. 19: VL9
72 Miller G D, Batchko R G, Tulloch W M, et al. 42%-efficient single-pass cw second-harmonic generation in periodically poled lithium niobate. Opt Lett, 1997, 22: 1834–1836
73 Ricciardi I, De Rosa M, Rocco A, et al. Cavity-enhanced generation of 6 W cw second-harmonic power at 532 nm in periodically-poled MgO:$LiTaO_3$. Opt Express, 2010, 18: 10985–10994
74 Pruneri V, Koch R, Kazansky P G, et al. 49 mW of cw blue light generated by first-order quasi-phase-matched frequency doubling of a diode-pumped 946-nm Nd:YAG laser. Opt Lett, 1995, 20: 2375
75 Batchko R G, Fejer M M, Byer R L, et al. Continuous-wave quasi-phase-matched generation of 60 mW at 465 nm by single-pass frequency doubling of a laser diode in backswitch-poled lithium niobate. Opt Lett, 1999, 24: 1293–1295
76 Xu P, Li K, Zhao G, et al. Quasi-phase-matched generation of tunable blue light in a quasi-periodic structure. Opt Lett, 2004, 29: 95–97
77 Vance J D, She C Y, Moosmüller H. Continuous-wave, all-solid-state, single-frequency 400-mW source at 589 nm based on doubly resonant sum-frequency mixing in a monolithic lithium niobate resonator. Appl Opt, 1998, 37: 4891–4896
78 Yue J, She C Y, Williams B P, et al. Continuous-wave sodium D_2 resonance radiation generated in single-pass sum-frequency generation with periodically poled lithium niobate. Opt Lett, 2009, 34: 1093–1095
79 Tracy A J, Lopez C, Hankla A, et al. Generation of high-average-power visible light in periodically poled nearly stoichiometric lithium tantalate. Appl Opt, 2009, 48: 964–968
80 Mimoun E, De Sarlo L, Zondy J J, et al. Sum-frequency generation of 589 nm light with near-unit efficiency. Opt Express, 2008, 16: 18684–18691
81 Georgiev D, Gapontsev V P, Dronov A G, et al. Watts-level frequency doubling of a narrow line linearly polarized Raman fiber laser to 589 nm. Opt Express, 2005, 13: 6772–6776
82 White R T, McKinnie I T, Butterworth S D, et al. Tunable single-frequency ultraviolet generation from a continuous-wave Ti: Sapphire laser with an intracavity PPLN frequency doubler. Appl Phys B, 2003, 77: 547–550
83 Mizuuchi K, Sugita T, Yamamoto K, et al. Efficient 340-nm light generation by a ridge-type waveguide in a first-order periodically poled MgO:$LiNbO_3$. Opt Lett, 2003, 28: 1344–1346
84 Meyn J P, Fejer M M. Tunable ultraviolet radiation by second-harmonic generation in periodically poled lithium tantalate. Opt Lett, 1997, 22: 1214–1216
85 Mizuuchi K, Yamamoto K. Generation of 340-nm light by frequency doubling of a laser diode in bulk periodically poled $LiTaO_3$. Opt Lett, 1996, 21: 107–109
86 Champert P A, Popov S V, Taylor J R, et al. Efficient second-harmonic generation at 384 nm in periodically poled lithium tantalate by use of a visible Yb-Er-seeded fiber source. Opt Lett, 2000, 25: 1252–1254
87 Liu Z W, Zhu S N, Zhu Y Y, et al. Quasi-Cw ultraviolet generation in a dual-periodic $LiTaO_3$ superlattice by frequency tripling. Jpn J Appl Phys, 2001, 40: 6841–6844
88 Wang S, Pasiskevicius V, Hellstrã M J, et al. First-order type II quasi-phase-matched UV generation in periodically poled KTP. Opt Lett, 1999, 24: 978–980
89 Wang S, Pasiskevicius V, Laurell F, et al. Ultraviolet generation by first-order frequency doubling in periodically poled $KTiOPO_4$. Opt Lett, 1998, 23: 1883–1885
90 Zhang B, Ding Y J, Zotova I B. Efficient ultrafast ultraviolet generation based on frequency doubling in short-period periodically-poled $KTiOPO_4$ crystal. Appl Phys B, 2010, 99: 629–632
91 Yamamoto K, Yamamoto H, Taniuchi T. Simultaneous sum-frequency and second-harmonic generation from a proton-exchanged MgO-doped $LiNbO_3$ waveguide. Appl Phys Lett, 1991, 58: 1227–1229
92 Cantelar E, Torchia G A, Sanz-Garcıa J A, et al. Red, green, and blue simultaneous generation in aperiodically poled Zn-diffused $LiNbO_3$: Er^{3+}/Yb^{3+} nonlinear channel waveguides. Appl Phys Lett, 2003, 83: 2991–2993

93 Capmany J. Simultaneous generation of red, green, and blue continuous-wave laser radiation in Nd^{3+}-doped aperiodically poled lithium niobate. Appl Phys Lett, 2001, 78: 144–146
94 Feng J, Zhu Y, Ming N. Harmonic generations in an optical Fibonacci superlattice. Phys Rev B, 1990, 41: 5578–5582
95 Zhu S. Quasi-phase-matched third-harmonic generation in a quasi-periodic optical superlattice. Science, 1997, 278: 843–846
96 Hu X P, Zhao G, Yan Z, et al. High-power red-green-blue laser light source based on intermittent oscillating dual-wavelength Nd:YAG laser with a cascaded $LiTaO_3$ superlattice. Opt Lett, 2008, 33: 408–410
97 Liu Z W, Zhu S N, Zhu Y Y, et al. A scheme to realize three-fundamental-colors laser based on quasi-phase matching. Solid State Commun, 2001, 119: 363–366
98 Xu P, Xie Z D, Leng H Y, et al. Frequency self-doubling optical parametric amplification: Noncollinear red-green-blue light-source generation based on a hexagonally poled lithium tantalate. Opt Lett, 2008, 33: 2791–2793
99 Zhao L, Qi Z, Yuan Y, et al. Integrated noncollinear red-green-blue laser light source using a two-dimensional nonlinear photonic quasicrystal. J Opt Soc Am B, 2011, 28: 608–612
100 Chang W K, Chen Y H, Chang H H, et al. Two-dimensional PPLN for simultaneous laser Q-switching and optical parametric oscillation in a Nd:YVO_4 laser. Opt Express, 2011, 19: 23643–23651
101 Xu P, Zhu S N. Review article: Quasi-phase-matching engineering of entangled photons. AIP Adv, 2012, 2: 041401
102 Ou Z Y, Mandel L. Violation of Bell's inequality and classical probability in a two-photon correlation experiment. Phys Rev Lett, 1988, 61: 50–53
103 Shih Y H, Alley C O. New type of einstein-podolsky-rosen-bohm experiment using pairs of light quanta produced by optical parametric down conversion. Phys Rev Lett, 1988, 61: 2921–2924
104 Bouwmeester D, Pan J W, Mattle K, et al. Experimental quantum teleportation. Nature, 1997, 390: 575–579
105 Pittman T B, Shih Y H, Strekalov D V, et al. Optical imaging by means of two-photon quantum entanglement. Phys Rev A, 1995, 52: R3429–R3432
106 Strekalov D V, Sergienko A V, Klyshko D N, et al. Observation of two-photon "ghost" interference and diffraction. Phys Rev Lett, 1995, 74: 3600–3603
107 Afek I, Ambar O, Silberberg Y. High-NOON states by mixing quantum and classical light. Science, 2010, 328: 879–881
108 Franson J D. Two-photon interferometry over large distances. Phys Rev A, 1991, 44: 4552–4555
109 Kwiat P G, Mattle K, Weinfurter H, et al. New high-intensity source of polarization-entangled photon pairs. Phys Rev Lett, 1995, 75: 4337–4341
110 Mair A, Vaziri A, Weihs G, et al. Entanglement of the orbital angular momentum states of photons. Nature, 2001, 412: 313–316
111 Grimau Puigibert M, Aguilar G H, Zhou Q, et al. Heralded single photons based on spectral multiplexing and feed-forward control. Phys Rev Lett, 2017, 119: 083601
112 Shalm L K, Hamel D R, Yan Z, et al. Three-photon energy-time entanglement. Nat Phys, 2012, 9: 19–22
113 Kuklewicz C E, Fiorentino M, Messin G, et al. High-flux source of polarization-entangled photons from a periodically poled $KTiOPO_4$ parametric down-converter. Phys Rev A, 2004, 69: 013807
114 Bao X H, Qian Y, Yang J, et al. Generation of narrow-band polarization-entangled photon pairs for atomic quantum memories. Phys Rev Lett, 2008, 101: 190501
115 Scholz M, Koch L, Benson O. Statistics of narrow-band single photons for quantum memories generated by ultrabright cavity-enhanced parametric down-conversion. Phys Rev Lett, 2009, 102: 063603
116 Xu C, Zhang L, Huang S, et al. Sensing and tracking enhanced by quantum squeezing. Photon Res, 2019, 7: A14
117 Vahlbruch H, Mehmet M, Danzmann K, et al. Detection of 15 dB squeezed states of light and their application for the absolute calibration of photoelectric quantum efficiency. Phys Rev Lett, 2016, 117: 110801
118 Liu F, Zhou Y, Yu J, et al. Squeezing-enhanced fiber Mach-Zehnder interferometer for low-frequency phase measurement. Appl Phys Lett, 2017, 110: 021106
119 Kaiser F, Fedrici B, Zavatta A, et al. A fully guided-wave squeezing experiment for fiber quantum networks. Optica, 2016, 3: 362–365
120 Sua Y M, Chen J Y, Huang Y P. Ultra-wideband and high-gain parametric amplification in telecom wavelengths with an optimally mode-matched PPLN waveguide. Opt Lett, 2018, 43: 2965–2968
121 Takesue H, Dyer S D, Stevens M J, et al. Quantum teleportation over 100 km of fiber using highly efficient superconducting nanowire single-photon detectors. Optica, 2015, 2: 832–835
122 Zhong T, Zhou H, Horansky R D, et al. Photon-efficient quantum key distribution using time-energy entanglement with high-dimensional encoding. New J Phys, 2015, 17: 022002
123 Zhang H, Jin X M, Yang J, et al. Preparation and storage of frequency-uncorrelated entangled photons from cavity-enhanced spontaneous parametric downconversion. Nat Photon, 2011, 5: 628–632
124 Gong Y X, Xie Z D, Xu P, et al. Compact source of narrow-band counterpropagating polarization-entangled photon pairs using a single dual-periodically-poled crystal. Phys Rev A, 2011, 84: 053825
125 Ueno W, Kaneda F, Suzuki H, et al. Entangled photon generation in two-period quasi-phase-matched parametric down-conversion. Opt Express, 2012, 20: 5508–5517
126 Zhang Q Y, Xue G T, Xu P, et al. Manipulation of tripartite frequency correlation under extended phase matchings. Phys Rev A, 2018, 97: 022327
127 Bai Y F, Xu P, Xie Z D, et al. Mode-locked biphoton generation by concurrent quasi-phase-matching. Phys Rev A, 2012, 85: 053807
128 Nasr M B, Carrasco S, Saleh B E A, et al. Ultrabroadband biphotons generated via chirped quasi-phase-matched optical parametric down-conversion. Phys Rev Lett, 2008, 100: 183601
129 Valencia A, Scarcelli G, Shih Y. Distant clock synchronization using entangled photon pairs. Appl Phys Lett, 2004, 85: 2655–2657
130 Giovannetti V, Lloyd S, Maccone L. Quantum-enhanced measurements: Beating the standard quantum limit. Science, 2004, 306: 1330–1336
131 Nasr M B, Saleh B E A, Sergienko A V, et al. Demonstration of dispersion-canceled quantum-optical coherence tomography. Phys Rev Lett, 2003, 91: 083601
132 Jin H, Liu F M, Xu P, et al. On-chip generation and manipulation of entangled photons based on reconfigurable lithium-niobate waveguide circuits. Phys Rev Lett, 2014, 113: 103601
133 Solntsev A S, Setzpfandt F, Clark A S, et al. Generation of nonclassical biphoton states through cascaded quantum walks on a nonlinear chip. Phys Rev X, 2014, 4: 031007
134 Krapick S, Brecht B, Herrmann H, et al. On-chip generation of photon-triplet states. Opt Express, 2016, 24: 2836–2849
135 Atzeni S, Rab A S, Corrielli G, et al. Integrated sources of entangled photons at the telecom wavelength in femtosecond-laser-written circuits. Optica, 2018, 5: 311–314
136 Shapira A, Naor L, Arie A. Nonlinear optical holograms for spatial and spectral shaping of light waves. Sci Bull, 2015, 60: 1403–1415
137 Arie A, Voloch N. Periodic, quasi-periodic, and random quadratic nonlinear photonic crystals. Laser Photon Rev, 2010, 4: 355–373
138 Hu X, Zhang Y, Zhu S. Nonlinear beam shaping in domain engineered ferroelectric crystals. Adv Mater, 2019, 1903775
139 Xu P, Ji S H, Zhu S N, et al. Conical second harmonic generation in a two-dimensional $\chi(2)$ photonic crystal: a hexagonally poled $LiTaO_3$ crystal. Phys Rev Lett, 2004, 93: 133904
140 Fang X, Wei D, Wang Y, et al. Conical third-harmonic generation in a hexagonally poled $LiTaO_3$ crystal. Appl Phys Lett, 2017, 110: 111105
141 Allen L, Beijersbergen M W, Spreeuw R J C, et al. Orbital angular momentum of light and the transformation of Laguerre-Gaussian laser modes. Phys Rev A, 1992, 45: 8185–8189

142 Simpson N B, Dholakia K, Allen L, et al. Mechanical equivalence of spin and orbital angular momentum of light: An optical spanner. Opt Lett, 1997, 22: 52–54
143 He H, Friese M E J, Heckenberg N R, et al. Direct observation of transfer of angular momentum to absorptive particles from a laser beam with a phase singularity. Phys Rev Lett, 1995, 75: 826–829
144 Padgett M, Bowman R. Tweezers with a twist. Nat Photon, 2011, 5: 343–348
145 Grier D G. A revolution in optical manipulation. Nature, 2003, 424: 810–816
146 Gibson G, Courtial J, Padgett M J, et al. Free-space information transfer using light beams carrying orbital angular momentum. Opt Express, 2004, 12: 5448–5456
147 Wang A, Zhu L, Chen S, et al. Characterization of LDPC-coded orbital angular momentum modes transmission and multiplexing over a 50-km fiber. Opt Express, 2016, 24: 11716–11726
148 Xiao S, Zhang L, Wei D, et al. Orbital angular momentum-enhanced measurement of rotation vibration using a Sagnac interferometer. Opt Express, 2018, 26: 1997–2005
149 Vaziri A, Pan J W, Jennewein T, et al. Concentration of higher dimensional entanglement: Qutrits of photon orbital angular momentum. Phys Rev Lett, 2003, 91: 227902
150 Shapira A, Shiloh R, Juwiler I, et al. Two-dimensional nonlinear beam shaping. Opt Lett, 2012, 37: 2136–2138
151 Lee W H. Binary computer-generated holograms. Appl Opt, 1979, 18: 3661–3669
152 Bloch N V, Shemer K, Shapira A, et al. Twisting light by nonlinear photonic crystals. Phys Rev Lett, 2012, 108: 233902
153 Shemer K, Voloch-Bloch N, Shapira A, et al. Azimuthal and radial shaping of vortex beams generated in twisted nonlinear photonic crystals. Opt Lett, 2013, 38: 5470–5473
154 Berry M V, Balazs N L. Nonspreading wave packets. Am J Phys, 1979, 47: 264–267
155 Siviloglou G A, Broky J, Dogariu A, et al. Observation of accelerating Airy beams. Phys Rev Lett, 2007, 99: 213901
156 Ellenbogen T, Voloch-Bloch N, Ganany-Padowicz A, et al. Nonlinear generation and manipulation of Airy beams. Nat Photon, 2009, 3: 395–398
157 Torres J P, Alexandrescu A, Carrasco S, et al. Quasi-phase-matching engineering for spatial control of entangled two-photon states. Opt Lett, 2004, 29: 376–378
158 Pittman T B, Strekalov D V, Klyshko D N, et al. Two-photon geometric optics. Phys Rev A, 1996, 53: 2804–2815
159 Boto A N, Kok P, Abrams D S, et al. Quantum interferometric optical lithography: Exploiting entanglement to beat the diffraction limit. Phys Rev Lett, 2000, 85: 2733–2736
160 Yu X Q, Xu P, Xie Z D, et al. Transforming spatial entanglement using a domain-engineering technique. Phys Rev Lett, 2008, 101: 233601
161 Leng H Y, Yu X Q, Gong Y X, et al. On-chip steering of entangled photons in nonlinear photonic crystals. Nat Commun, 2011, 2: 429
162 Jin H, Xu P, Zhao J S, et al. Observation of quantum Talbot effect from a domain-engineered nonlinear photonic crystal. Appl Phys Lett, 2012, 101: 211115
163 Barbieri M, De Martini F, Mataloni P, et al. Enhancing the violation of the einstein-podolsky-rosen local realism by quantum hyper-entanglement. Phys Rev Lett, 2006, 97: 140407
164 Barreiro J T, Langford N K, Peters N A, et al. Generation of hyperentangled photon pairs. Phys Rev Lett, 2005, 95: 260501
165 Chen K, Li C M, Zhang Q, et al. Experimental realization of one-way quantum computing with two-photon four-qubit cluster states. Phys Rev Lett, 2007, 99: 120503
166 Rossi A, Vallone G, Chiuri A, et al. Multipath entanglement of two photons. Phys Rev Lett, 2009, 102: 153902
167 Megidish E, Halevy A, Eisenberg H S, et al. Compact 2D nonlinear photonic crystal source of beamlike path entangled photons. Opt Express, 2013, 21: 6689–6696
168 Jin H, Xu P, Luo X W, et al. Compact engineering of path-entangled sources from a monolithic quadratic nonlinear photonic crystal. Phys Rev Lett, 2013, 111: 023603
169 Liu H Y, Zhang R, Xu P, et al. Compact generation of a two-photon multipath Dicke state from a single $\chi^{(2)}$ nonlinear photonic crystal. Opt Lett, 2019, 44: 239–242
170 Gong Y X, Xu P, Shi J, et al. Generation of polarization-entangled photon pairs via concurrent spontaneous parametric down-conversions in a single $\chi^{(2)}$ nonlinear photonic crystal. Opt Lett, 2012, 37: 4374–4376
171 Lu L L, Xu P, Zhong M L, et al. Orbital angular momentum entanglement via fork-poling nonlinear photonic crystals. Opt Express, 2015, 23: 1203–1212
172 Ming Y, Tang J, Chen Z X, et al. Generation of N00N state with orbital angular momentum in a twisted nonlinear photonic crystal. IEEE J Sel Top Quantum Electron, 2015, 21: 225–230
173 He G, Zhu C, Jiang Y, et al. Generation of path-polarization hyperentanglement using quasi-phase-matching in quasi-periodic nonlinear photonic crystal. Sci Rep, 2017, 7: 4954
174 Ihlefeld J F, Michael J R, McKenzie B B, et al. Domain imaging in ferroelectric thin films via channeling-contrast backscattered electron microscopy. J Mater Sci, 2016, 52: 1071–1081
175 Kläui M, Ehrke H, Rüdiger U, et al. Direct observation of domain-wall pinning at nanoscale constrictions. Appl Phys Lett, 2005, 87: 102509
176 Gonnissen J, Batuk D, Nataf G F, et al. Direct observation of ferroelectric domain walls in $LiNbO_3$: Wall-meanders, kinks, and local electric charges. Adv Funct Mater, 2016, 26: 7599–7604
177 Sawada A, Abe R. The formation mechanism of domain etch patterns in triglycine sulfate crystals. Jpn J Appl Phys, 1967, 6: 699–707
178 Talbot H F. LXXVI. Facts relating to optical science. No. IV. London Edinburgh Dublin Philos Mag J Sci, 1836, 9: 401–407
179 Zhang Y, Wen J, Zhu S N, et al. Nonlinear Talbot effect. Phys Rev Lett, 2010, 104: 183901
180 Wei D, Wang C, Xu X, et al. Efficient nonlinear beam shaping in three-dimensional lithium niobate nonlinear photonic crystals. Nat Commun, 2019, 10: 4193
181 Liu S, Switkowski K, Xu C, et al. Nonlinear wavefront shaping with optically induced three-dimensional nonlinear photonic crystals. Nat Commun, 2019, 10: 3208
182 Lu R E, Zhao R Z, Feng X, et al. Nearly diffraction-free nonlinear imaging of irregularly distributed ferroelectric domains. Phys Rev Lett, 2018, 120: 067601
183 Ducournau G. Silicon photonics targets terahertz region. Nat Photon, 2018, 12: 574–575